Available online at www.sciencedirect.com
ScienceDirect
Trans. Nonferrous Met. Soc. China 32(2022) 1866−1880
Transactions of Nonferrous Metals Society of China
www.tnmsc.cn

# Mechanical properties of Mg−Gd−Zr alloy by Nd addition combined with hot extrusion

Liu-wei ZHENG[1], Yong-peng ZHUANG[1], Jun-jian LI[1], Hong-xia WANG[1],
Hang LI[1], Hua HOU[2], Li-fei WANG[1], Xiao-ping LUO[1], Kwang Seon SHIN[3]

1. Shanxi Key Laboratory of Advanced Magnesium based Materials,
College of Materials Science and Engineering, Taiyuan University of Technology, Taiyuan 030024, China;
2. School of Materials Science and Engineering, North University of China, Taiyuan 030051, China;
3. Magnesium Technology Innovation Center, School of Materials Science and Engineering,
Seoul National University, Seoul-08826, Korea

Received 9 June 2021; accepted 20 February 2022

**Abstract:** The effect of Nd addition on the microstructure and mechanical properties of as-extruded Mg−9Gd−0.5Zr (wt.%) alloy was investigated. The Mg−9Gd−0.5Zr and Mg−9Gd−2Nd−0.5Zr alloys were extruded at 673 K. The elongated non-dynamic recrystallized (un-DRXed) grains disappear after adding Nd, and uniformly distributed dynamic recrystallized grains with a grain size of 1.68 μm were obtained in the alloy. In addition, numerous nano-$Mg_5$(Gd,Nd) particles were found to precipitate dynamically in the Mg−9Gd−2Nd−0.5Zr alloy, which gave rise to the dynamic recrystallization process via providing nucleation energy through hindering the release of deformation energy and promoting an increase in the strength through the Orowan strengthening mechanism. Moreover, the dynamically recrystallized (DRXed) grains have a weak texture, which plays a significant role in improving the ductility. Therefore, the Nd addition favors the improvement of strength and elongation for the as-extruded Mg−9Gd−0.5Zr alloy, simultaneously.

**Key words:** Mg−Gd based alloy; hot extrusion; DRX behavior; texture; mechanical properties

## 1 Introduction

Due to their low density, high specific strength and good casting performance, Mg alloys are widely used in the automobile and aerospace industries [1−3]. As an efficient, economical and advanced processing method for wrought magnesium alloys, hot extrusion can significantly improve the mechanical properties of magnesium alloys through promoting the precipitation of the second phase and refining the grain size of the alloy [4−8]. For example, YU et al [9] developed extruded Mg−11Gd−4.5Y−1Nd−1.5Zn−0.5Zr (wt.%) alloy with a yield strength of 306 MPa, which was attributed to many fine dispersed $Mg_5RE$ precipitates and high-volume fraction dynamic recrystallization. LIU et al [10] manufactured a Mg−5Zn−1Ce−0.5Y−0.6Zr alloy with excellent yield strength (389 MPa) only by extrusion. However, these extruded alloys exhibit poor plasticity (<10%). This was mainly due to the formation of a $\langle 2\bar{1}\bar{1}0\rangle$ - $\langle 11\bar{2}0\rangle$ double fiber texture after extrusion, which evolved from the prismatic $\langle 2\bar{1}\bar{1}0\rangle$ fiber texture. The base plane of this texture is parallel to the extrusion direction, which is not conducive to the initiation of base plane slip, thus limiting the improvement of plasticity [11].

**Corresponding author:** Hong-xia WANG, Tel: +86-13233686858, E-mail: wanghxia1217@163.com;
Yong-peng ZHUANG, Tel: +86-15333017947, E-mail: 1078408347@qq.com
DOI: 10.1016/S1003-6326(22)65914-4

In recent years, some studies have shown that the addition of rare earth element (Gd, Ce, Y, Nd) can improve the ductility of wrought magnesium alloys due to the formation of the rare earth texture [12−15]. Among them, Mg−Gd based alloys have been widely concerned because of their excellent properties at elevated temperatures [16−19]. Recently, a Mg−14Gd−0.5Zr (wt.%) alloy with a yield strength of 190 MPa and an elongation of 19.5% was prepared by extrusion [20]. A Mg−Gd−Zn−Zr alloy with excellent elongation higher than 23% was produced by LIU et al [21] through extrusion. Although the plasticity of Mg−Gd alloy is improved by extrusion, its strength needs to be improved further.

Nd is selected to be added to Mg−Gd based alloys because of the formation of RE texture during extrusion. Moreover, Gd and Nd belong to different rare earth group systems (cerium group and yttrium group) [22], which reduces their solid solution degrees to each other in Mg to promote the formation of the second phase. Thus, abundant broken second phases (>1 μm) will be formed during extrusion, which promotes precipitation through the particle-stimulated nucleation (PSN) effect, resulting in higher strength [8]. In addition, it has been reported that PSN is an active mechanism for dynamic recrystallization (DRX) which contributes to the development of a weaker texture during extrusion [23,24].

However, there are many nano second phases precipitating from the matrix during extrusion, which cannot promote recrystallization through the PSN effect due to the size being less than 1 μm. There are few studies on the effect of nano precipitates on the recrystallization behavior of alloys. Therefore, in the present work, a Mg−Gd based alloy with Nd addition was extruded. The effect of Nd addition on the microstructure and mechanical properties of Mg−9Gd−0.5Zr alloy during extrusion, especially the texture, was studied. And, the interaction between the second phase and recrystallization was explored in details.

## 2 Experimental

The Mg−9Gd−0.5Zr (wt.%) and Mg−9Gd−2Nd−0.5Zr (wt.%) alloys were prepared by using pure Mg (99.9 wt.%), pure Gd (99.99 wt.%), Mg−30Nd (wt.%) master alloy and Mg−30Zr (wt.%) master alloy. The raw materials were melted in an electrical furnace at 1053 K for 60 min under the $SF_6/CO_2$ (1:99 of volume ratio) protective gas and then poured into a steel mold with an inner diameter of 40 mm preheated to 473 K. The shape of the as-cast alloy is cylindrical and the size is *d*40 mm × 150 mm. The chemical compositions of the experimental alloys were determined by inductively-coupled plasma (ICP) and the results are listed in Table 1. The homogenization treatment was carried out at 798 K for 4 h and sequenced by water quenching at 298 K. The homogenized ingot was machined into *d*40 mm × 50 mm cylindrical extrusion billet. The extrusion was performed at 673 K with an extrusion ratio of 16:1 and at a ram speed of 30 mm/min. Before extrusion, the billet was preheated to 673 K and held for 30 min to reach the extrusion temperature.

**Table 1** Chemical compositions of experimental alloys determined by ICP (wt.%)

| Alloy | Gd | Nd | Zr | Mg |
|---|---|---|---|---|
| Mg−9Gd−0.5Zr | 9.03 | − | 0.58 | Bal. |
| Mg−9Gd−2Nd−0.5Zr | 8.95 | 2.07 | 0.52 | Bal. |

The microstructure of the alloy was observed by optical microscopy (OM) using a Leica 2700M light optical microscope. A TESCAN Mira3 LMH scanning electron microscope (SEM) equipped with energy dispersive spectrometry (EDS) was used to identify the composition of the second phase. The scanning voltage was 10 kV and the current was 10 mA. The OM and SEM samples were polished with sandpaper until there was no obvious scratch, then polished, finally etched by 4% nitric acid alcohol. The observation position of the as-cast alloy was in the center of the cylinder 10 mm from the bottom. The electron back scattered diffraction (EBSD) specimen was mechanically polished and sequenced by electrolytic polishing using ACII solution. The EBSD measurement (voltage 15 keV, step size 0.3 μm) was used to characterize the local microstructure and texture by TESCAN S8000. To ensure statistical rigor, more than 1000 grains were examined for each condition. The EBSD data were analyzed using Channel 5.0 Analysis software. In the bimodal microstructure, the DRXed and un-DRXed grains were distinguished according to the average grain misorientation of the EBSD data. The tensile test was carried out on a universal testing machine (WDW−100KN) at room temperature. The shape of the tensile sample was bony, the gauge sizes were 2 mm × 4 mm × 18 mm, and the tensile speed was 0.2 mm/min. The sampling position of the tensile test bar was selected in the center of the as-cast and as-extruded alloys along the extrusion direction (ED). Each state was tested at least three times.

## 3 Results and discussion

### 3.1 Microstructure before extrusion

As shown in Fig. 1, the microstructures of the as-cast Mg−9Gd−(2Nd)−0.5Zr alloys mainly consist of $\alpha$-Mg matrix (marked by *A*), skeletal second phase distributed at grain boundaries (marked by *B* and *D*) and square phase (marked by *C* and *E*). In addition, there are Gd-rich regions around the skeletal second phase due to the composition segregation during solidification. According to the EDS results listed in Table 2, the skeleton phase is $Mg_5Gd$ phase in the Mg−9Gd−0.5Zr alloy. While, with the addition of Nd, the $Mg_5Gd$ phase is changed into the $Mg_5$(Gd,Nd) phase, that is, some Gd in $Mg_5Gd$ is replaced by Nd element. In addition, the $Mg_5$(Gd,Nd) phase in the alloy presents a discontinuous network structure. The fraction of Gd (and Nd) in the square phase is more than 80 wt.%, which is similar to the derivative phase of $Gd_2H$ previously reported [25,26]. Its formation is related to the dissolution of hydrogen element from the external environment. According to the statistics, the grain size of the alloy decreases after adding Nd, which is 48.75 and 41.21 μm, respectively.

It can be seen from Fig. 2 that the grains tend to be equiaxed after homogenization treatment, and the $Mg_5$(Gd,Nd) phase is resolved into the $\alpha$-Mg matrix. However, some $Mg_5Gd$ phase remains at the grain boundaries in the Mg−9Gd−0.5Zr alloy, which is mainly due to its high melting point. To analyze the element distribution of the solute atoms, energy dispersive X-ray spectroscopy (EDS) elemental mapping is conducted in the square area, as shown in Figs. 2(b, e). In the EDS maps, the elements were evenly distributed in the Mg−9Gd−2Nd−0.5Zr alloy, while the Gd element was aggregated in the white region in the Mg−9Gd−0.5Zr alloy. After homogenization treatment, the average grain size is 59.68 μm for the Mg−9Gd−0.5Zr alloy. Nevertheless, the grain sizes decrease after adding Nd, which is 47.62 μm for the Mg−9Gd−2Nd−0.5Zr alloy. There are two reasons for the decrease in grain size. One is mainly due to the heredity of grain size of the as-cast alloys [27]. On the other hand, more atoms are resolved into

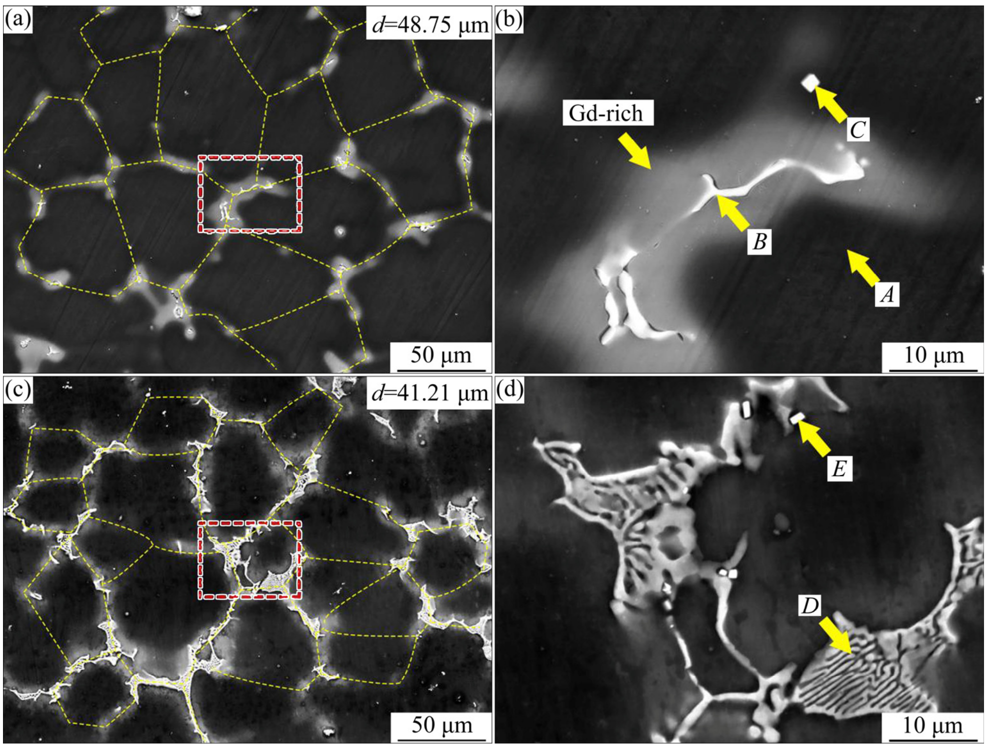


**Fig. 1** SEM images of as-cast alloys: (a, b) Mg−9Gd−0.5Zr, (c, d) Mg−9Gd−2Nd−0.5Zr

**Table 2** EDS analysis of matrix and second phases shown in Figs. 1(b) and (d) (at.%)

| Location | Mg | Gd | Nd | Zr | Phase |
|---|---|---|---|---|---|
| *A* | 98.6 | 1.3 | − | 0.1 | $\alpha$-Mg |
| *B* | 82.2 | 17.8 | − | − | $Mg_5Gd$ |
| *C* | 14.3 | 85.7 | − | − | $Gd_2H$ |
| *D* | 82.3 | 16.3 | 1.4 | − | $Mg_5(Gd,Nd)$ |
| *E* | 8.5 | 88.4 | 3.1 | − | $Gd_2H$ |

the matrix after homogenization treatment in the Mg−9Gd−2Nd−0.5Zr alloy, which has a strong drag effect on grain growth.

### 3.2 Microstructure after extrusion

The microstructures of Mg−9Gd−0.5Zr alloys with and without Nd after extrusion were observed by optical microscopy and scanning electron microscopy (Fig. 3). Figure 3(a) shows that the as-extruded Mg−9Gd−0.5Zr alloy presents a typical bimodal microstructure, which contains fine dynamically recrystallized grains and coarse un-DRXed grains elongated along the extrusion direction (marked by yellow circle). In contrast to the Mg−9Gd−0.5Zr alloy, the Mg−9Gd−2Nd−0.5Zr alloy has distinctly different microstructures. It is difficult to observe the coarse un-DRXed grains in the Mg−9Gd−2Nd−0.5Zr alloy, and the microstructure of the alloy is composed of fine dynamic recrystallized grains. Comparing Figs. 3(c) with (d), the grain size of the extruded Mg−9Gd−2Nd−0.5Zr alloy is smaller than that of the Mg−9Gd−0.5Zr alloy. In addition, in the Mg−9Gd−0.5Zr alloy, there are few broken second phases (>1 μm), which are surrounded by fine DRXed grains, indicating that the broken second phase (>1 μm) can promote dynamic recrystallization nucleation through the PSN effect. While, as shown in Fig. 3(d), it is not difficult to find that there are two kinds of recrystallized grain with different grain sizes (coarse and fine DRXed grains). And, there are few precipitates at the coarse recrystallized grain boundaries. However, extensive tiny precipitates (<1 μm) are observed at the fine DRXed grain boundaries. This indicates that during the extrusion process, the precipitates at the grain boundary can prevent the movement of grain boundary, thus control the size of the DRXed grains. To better observe the distribution of the second phase in the alloy, the microstructures of alloys without etching are exhibited in Figs. 3(e, f). In the Mg−9Gd−0.5Zr alloy, the broken second phase is distributed in strip along the extrusion direction, which is residual $Mg_5Gd$ after homogenization treatment. In addition, the dynamic precipitated second phase cannot be observed in Fig. 3(e). Compared with the Mg−9Gd−0.5Zr alloy, many precipitated second phases are observed in the Mg−9Gd−2Nd−0.5Zr alloy and are distributed evenly, indicating that the addition of Nd can promote the precipitation of the second phase during extrusion. It has been reported that the solid

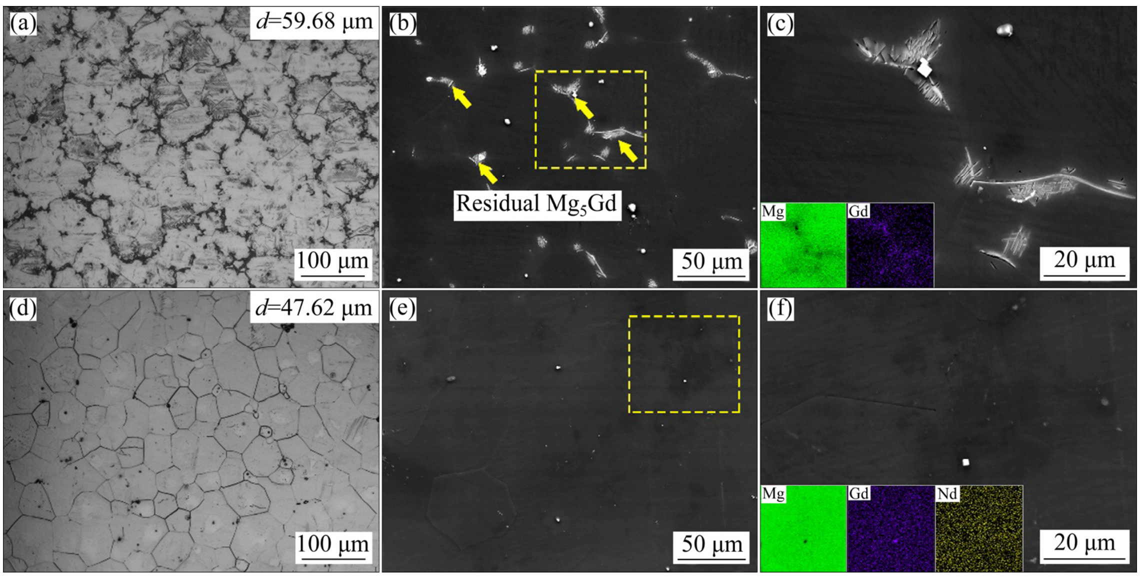


**Fig. 2** OM and SEM images and EDS maps of alloys after homogenization treatment: (a, b, c) Mg−9Gd−0.5Zr; (d, e, f) Mg−9Gd−2Nd−0.5Zr

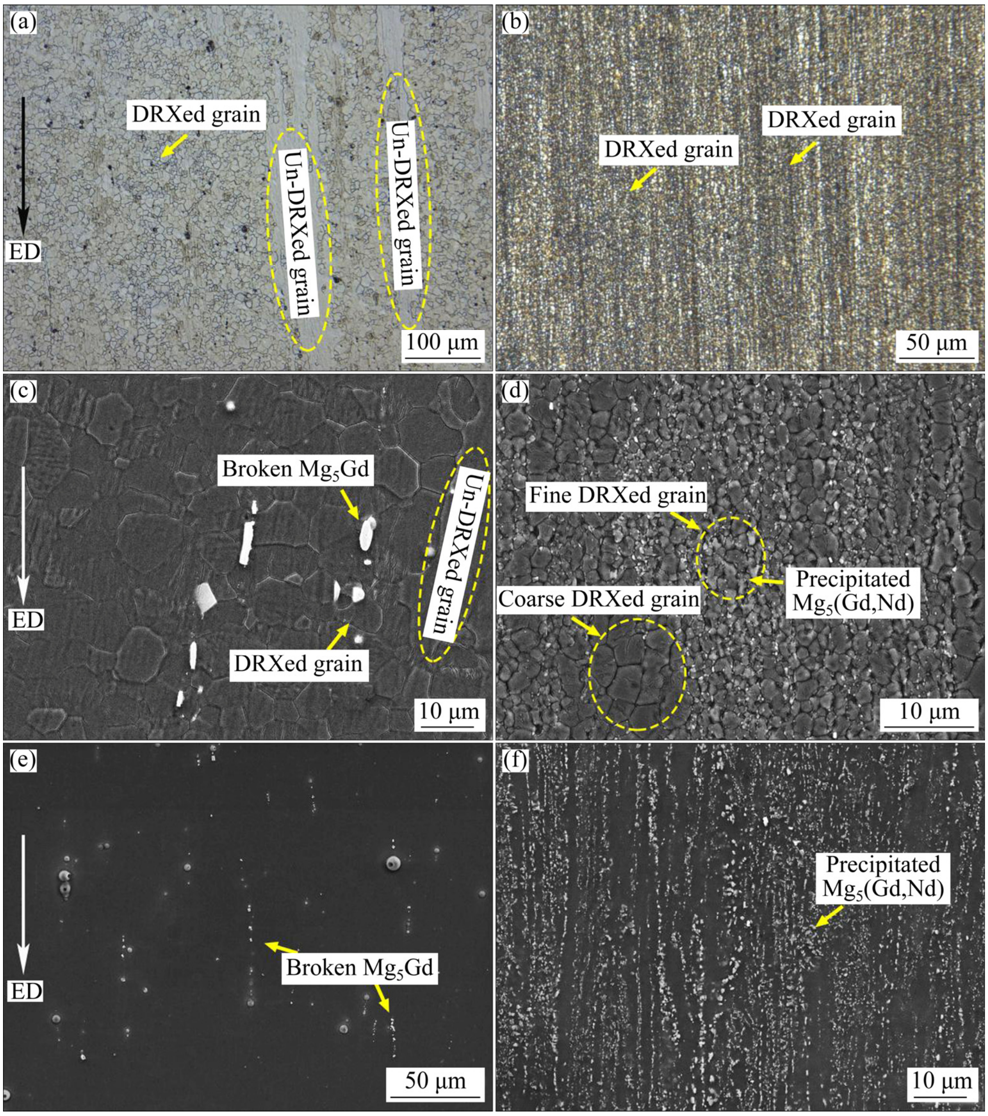


**Fig. 3** OM and SEM images of alloys after extrusion: (a, c, e) Mg−9Gd−0.5Zr; (b, d, f) Mg−9Gd−2Nd−0.5Zr

solubility of Gd atoms will be reduced in Mg when Nd is added at the same time [28]. Hence, the volume fraction of the second phase in the as-extruded Mg−9Gd−2Nd−0.5Zr alloy increases sharply.

The XRD analysis of the Mg−9Gd−(2Nd)−0.5Zr alloys under different conditions was carried out to reveal the evolution and crystal orientation of phase, and the results are shown in Fig. 4. The $Mg_5Gd$ and $Mg_5(Gd,Nd)$ phases share the same diffraction peak owing to the same crystal lattice structure (FCC) and similar lattice. It is obvious that the diffraction intensities on the (333) and (533) crystal planes of the $Mg_5RE$ phase decrease after homogenization treatment, especially in the Mg−9Gd−2Nd−0.5Zr alloy. This indicates that the quantity of the $Mg_5RE$ phase decreases after homogenization treatment, which is consistent with the previously observed results. Compared with the homogenized alloys, the diffraction intensities of the as-extruded Mg−9Gd−0.5Zr and Mg−9Gd−2Nd−0.5Zr alloys show completely different trends. The diffraction intensity of the as-extruded Mg−9Gd−0.5Zr alloy is similar to that of the homogenized Mg−9Gd−0.5Zr alloy, which shows that the quantity of $Mg_5Gd$ in the alloy is basically unchanged before and after extrusion. In the as-extruded Mg−9Gd−2Nd−0.5Zr alloy, the diffraction intensity on (533) plane increases considerably due to the large number of precipitated $Mg_5(Gd,Nd)$ phases after extrusion. In addition, it is worth noting that high diffraction intensities lie on the $(11\bar{2}0)$, $(10\bar{1}2)$ and $(11\bar{2}2)$ planes of $\alpha$-Mg, which indicates that grain twisting is promoted by hot extrusion resulting in increasing deformability [29].

The structures of Mg−9Gd−(2Nd)−0.5Zr alloys after extrusion were explored by EBSD observation to study the main recrystallization mechanisms. The EBSD maps of the extruded alloys are exhibited in Figs. 5(a, b). As can be seen from the maps, the elongated un-DRXed grains (blue grains) disappear

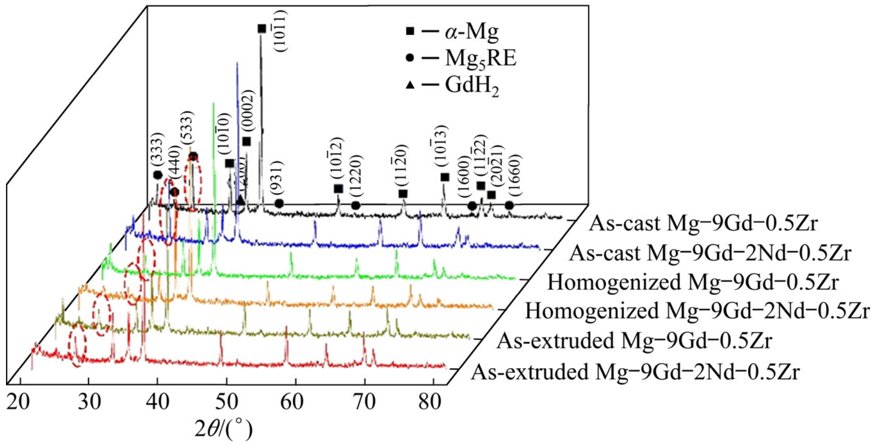


**Fig. 4** XRD patterns of Mg−9Gd−(2Nd)−0.5Zr alloys

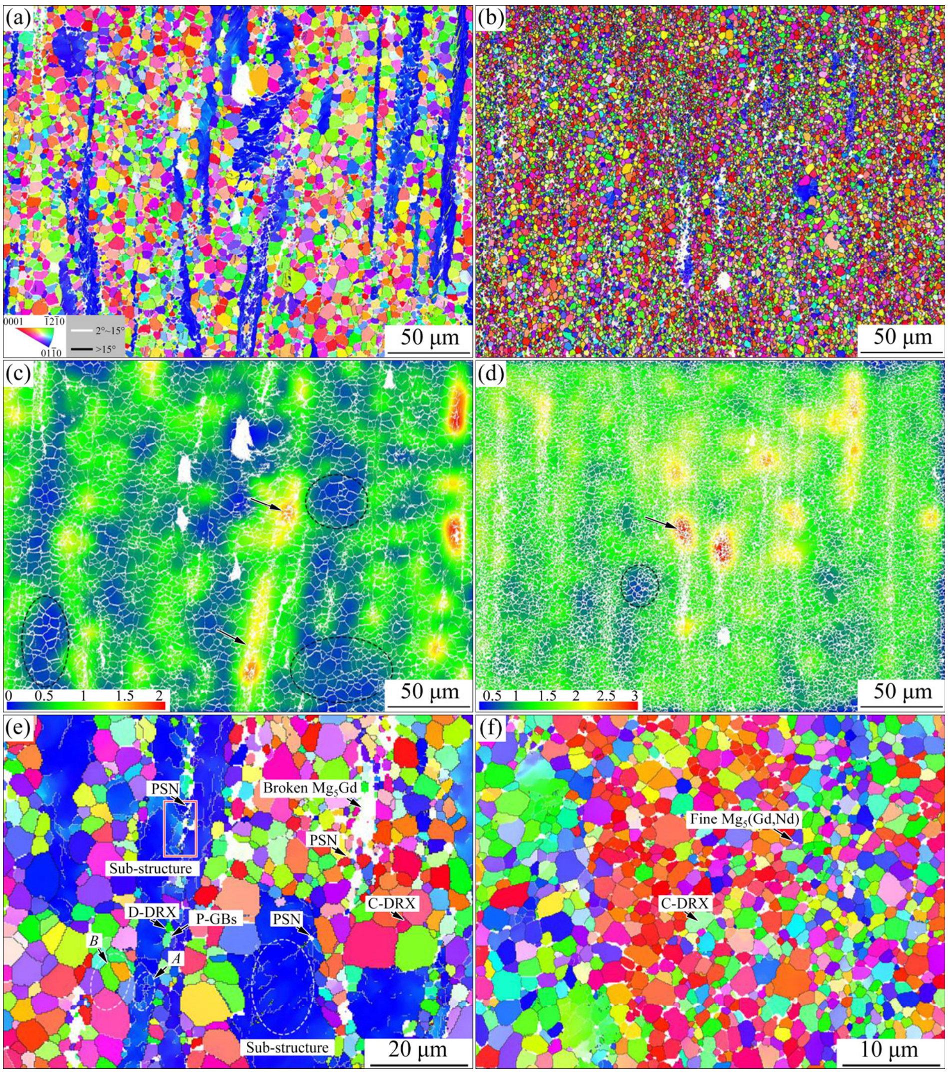


**Fig. 5** EBSD maps (a, b, e, f) and strain distribution maps (c, d) of alloys after extrusion: (a, c, e) Mg−9Gd−0.5Zr; (b, d, f) Mg−9Gd−2Nd−0.5Zr

after Nd addition, which is consistent with the optical microscopy observations. In addition, the subgrain structures with low-angle grain boundaries (<15°, LAGBs) are formed in the un-DRXed regions, as shown in Fig. 5(a). The average DRXed grain size ($\bar{d}_{\mathrm{DRX}}$) for the Mg−9Gd−0.5Zr alloy is 5.23 μm. When 2 wt.% Nd was added to the Mg−9Gd−0.5Zr alloy, the grain size rapidly decreased to 1.68 μm. The strain contouring maps (Figs. 5(c, d)) show the degree of lattice strain of each grain in the EBSD maps. The red area in the figure represents the area possessing the large lattice strain, indicating that large amounts of residual stress remains in the matrix. However, the blue area represents the area with less residual stress. In the Mg−9Gd−0.5Zr alloy, the region with high residual stress is mainly concentrated in the regions with broken second phases and the un-DRXed grains (marked by arrows in Fig. 5(c)). In the regions with broken second phases, there is a lattice misfit between the $\alpha$-Mg matrix and broken second phases due to their high stiffness and brittleness resulting in high residual stress. In the un-DRXed grains regions, the residual stress cannot be effectively released through recrystallization behavior. However, the residual stress in the recrystallization region (blue region) is small, indicating that the strain energy can be released by dynamic recrystallization. After adding 2 wt.% Nd, the high residual stress regions increase a lot in the alloy, and the strain value (SV) is mainly concentrated in the range of 1.1−1.4. The residual stress is mainly concentrated in the area with more precipitates and is small, where there are few precipitates and the recrystallized grains are large (marked by circle in Fig. 5(d)). This is because although recrystallization can release part of the stress, the growth of recrystallization is restrained in the region with more precipitates during extrusion, and the strain cannot be released, thus more stress concentration occurs in this region. However, in the region with few precipitates, the movement of grain boundaries is not impeding, which leads to significant stress relief. According to the KJMA relation, the nucleation rate ($n$) of dynamic recrystallization has a considerable relationship with the effective plastic strain $\varepsilon_{\mathrm{eff}}^{\mathrm{P}}$ in the following form [30]:

$$n = c\varepsilon_{\mathrm{eff}}^{\mathrm{P}} \exp[Q_{\mathrm{n}}/(RT)] \quad (1)$$

where $c$ is a constant, $Q_{\mathrm{n}}$ represents the activation energy for nucleation, $R$ represents the molar gas constant, and $T$ is the thermodynamic temperature. Therefore, the rate of nucleation is proportional to the plastic strain, which is proportional to the lattice strain. Based on the measurement, the average lattice strain value is 0.52 for the Mg−9Gd−0.5Zr alloy, and 1.25 for the Mg−9Gd−2Nd−0.5Zr alloy. This indicates that the plastic strain is large after Nd addition, which gives rise to dynamic recrystallization process through providing nucleation energy.

In order to further explore the recrystallization mechanism, high resolution EBSD observations were implemented (Figs. 5(e, f)). In the Mg−9Gd−0.5Zr alloy, many new grains are formed by discontinuous DRX (D-DRX) mechanism around the prior grain boundaries (P-GBs), which is due to the migration of large angle grain boundaries [31]. As shown in Fig. 5(e), some LAGBs cluster around the broken second phase as indicated by the red square, illustrating that the bulk broken $Mg_5Gd$ phase can promote the formation of new grains through the PSN mechanism due to the stress concentration occurring at the Mg/$Mg_5RE$ interface. In addition, some deformed grains are divided into several sub-grains by LAGBs (marked by $A$) to release the stored strain energy. During the extrusion process, the sub-GBs moved easily because there were no particles around them leading to coarsening of the sub-grains. Moreover, the misorientation between adjacent sub-grains increases, which leads to LAGBs transforming into high-angle grain boundaries (HAGBs). Eventually, coarse recrystallized grains form (marked by $B$) as a result of sub-GB evolution. This dynamic recrystallization process is considered as continuous DRX (C-DRX) [32]. In contrast to the Mg−9Gd−0.5Zr alloy, abundant nano second phases precipitated dynamically at the sub-GBs, which prevented the sub-GBs from sliding effectively, resulting in fine recrystallized grains. According to the analysis results from the inverse pole figures (IPFs) (Table 3), the fraction of LAGBs ($F_{\mathrm{LAGBs}}$) decreases significantly after adding 2 wt.% Nd, indicating that more LAGBs transform into HAGBs in the Mg−9Gd−2Nd−0.5Zr alloy. Consequently, in the Mg−9Gd−2Nd−0.5Zr alloy, the DRX process is more pronounced than that in the Mg−9Gd−0.5Zr alloy because numerous second phases precipitate during extrusion.

The IPFs of the studied alloys are presented in Fig. 6, including all grains, DRXed grains and un-DRXed grains. As can be seen from Fig. 6, the DRXed grains have a weak texture with a texture component between [0001] and $[\bar{1}2\bar{1}0]$, which is reported as RE texture [15,33]. Based on detection, the RE texture peak is approximately 30° from $[\bar{1}2\bar{1}0]$, which is $[\bar{1}2\bar{1}1]$. In addition to the RE texture component, there is a new texture peak at [0001] in the Mg−9Gd−2Nd−0.5Zr alloy. Alternatively, the un-DRXed grains exhibit a strong texture larger than 20, and the texture component is mainly concentrated in $[01\bar{1}0]$, that is, the un-DRXed grains are oriented with $[01\bar{1}0]$ parallel to the ED. As observed in all grains IPF, it is apparent that the maximum intensity decreases with the addition of Nd, which are 5.66 and 1.86 for Mg−9Gd−0.5Zr and Mg−9Gd− 2Nd−0.5Zr alloys, respectively. In the Mg−9Gd− 0.5Zr alloy, the texture of the un-DRXed grains dominates the grains texture. Due to the high DRX fraction ($F_{DRX}$=93.5%), all grain textures exhibit RE texture after adding Nd. Hence, the decrease in the texture intensity is related to the increase in the DRX fractions.

According to the above observation, the sketch map of the evolution of DRX during extrusion is shown in Fig. 7. In the Mg−9Gd−0.5Zr alloy, during the early stage of extrusion, dynamic recrystallization is formed. As the extrusion proceeds, the DRX grows up because there is little broken $Mg_5Gd$ phase which has a limited hindering effect on the grain boundary sliding. While in the Mg−9Gd−2Nd−0.5Zr alloy, numerous second phases precipitate dynamically at the recrystallized grain boundaries, which provides energy for the formation of dynamic recrystallization due to the hindrance of stress relief, resulting in larger amounts of residual stresses remaining in the matrix. In addition, the smaller DRXed grains have more grain boundaries, which provides more nucleation points for the precipitation of the second phase [34]. In summary, the formation of the dynamic recrystallization and the precipitation of the second phase are complementary in the extrusion process. Consequently, very fine dynamically recrystallized grains are formed and the second phase uniformly precipitates in the Mg−9Gd−2Nd−0.5Zr alloy.

### 3.3 Mechanical properties

The strengthening of the wrought magnesium alloy is mainly attributed to grain refinement, second phase particles and texture. The Mg−9Gd−0.5Zr alloy exhibited a bimodal structure consisting of DRXed grains with a fine grain size (5.23 μm) and elongated deformed grains. However, after adding Nd, the structure of the alloy mainly comprises DRXed grains and the size is refined to

**Table 3** Analysis results from IPF maps

| Alloy | SF | SV | $F_{LAGBs}$/% | $F_{Mg_5RE}$ /% | $F_{DRX}$/% | $\bar{d}_{DRX}$ /μm |
|---|---|---|---|---|---|---|
| Mg−9Gd−0.5Zr | 0.32 | 0.52 | 50.38 | 1.2 | 77.2 | 5.23 |
| Mg−9Gd−2Nd−0.5Zr | 0.33 | 1.25 | 12.06 | 10.4 | 93.5 | 1.68 |

$F_{Mg_5RE}$: Volume fraction of $Mg_5RE$ phase

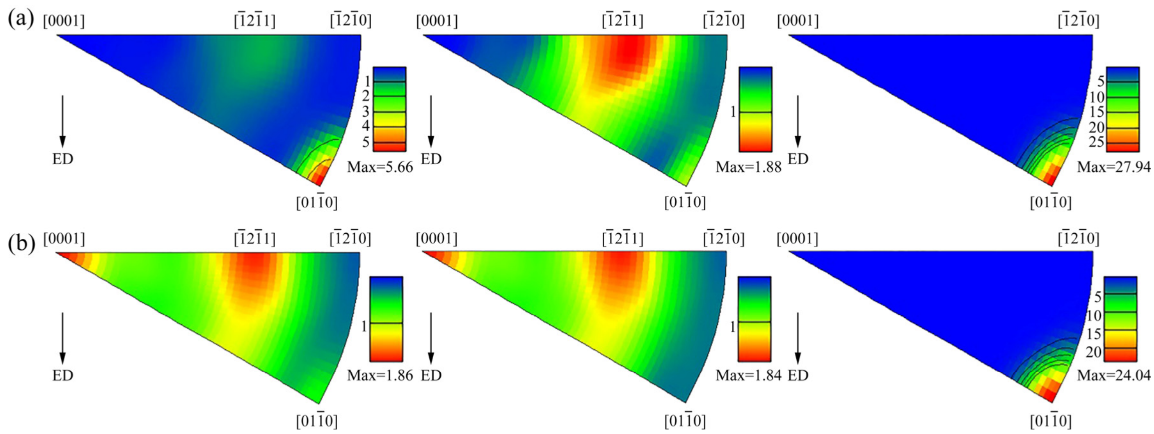


**Fig. 6** IPF maps of alloys after extrusion: (a) Mg−9Gd−0.5Zr; (b) Mg−9Gd−2Nd−0.5Zr

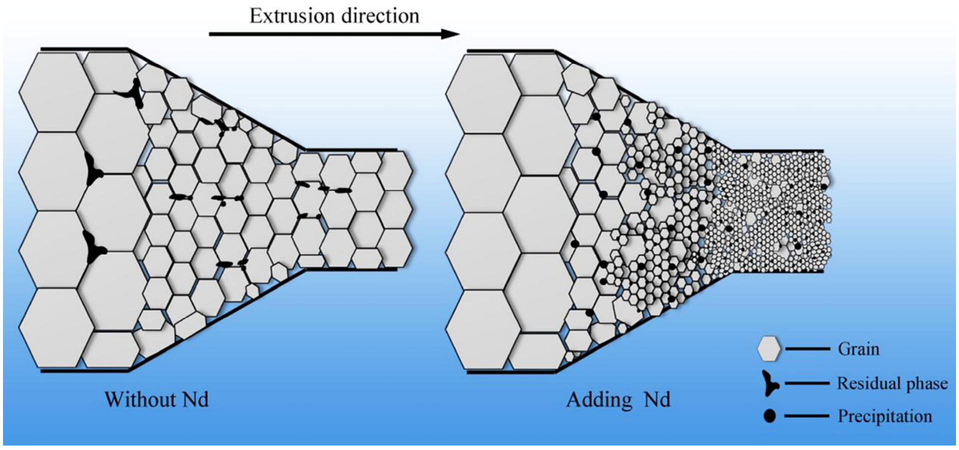


**Fig. 7** Evolution of DRX during extrusion

1.68 μm, which can improve the yield strength (YS) of the alloy to some extent through grain boundary strengthening according to the Hall−Petch relationship. Furthermore, a large amount of the second phase precipitates during the extrusion, which also contributes to the strengthening of the Mg−9Gd−2Nd−0.5Zr alloy. The tensile stress and strain curves of the as-cast and extruded Mg−9Gd−(2Nd)−0.5Zr alloys are exhibited in Fig. 8(a). According to Fig. 8(a), the tensile properties of the Mg−9Gd−(2Nd)−0.5Zr alloys under different conditions are summarized in Fig. 8(b). It is evident that, after extrusion, the strength and elongation of the studied alloys increase simultaneously compared with those of the as-cast alloys. Compared with the as-cast alloy, the yield strength of the extruded Mg−9Gd−0.5Zr increases by 111.5 MPa, which is due to the fine grain size after extrusion. For the Mg−9Gd−2Nd−0.5Zr alloy, the improvement in YS increases to 216.2 MPa. In addition to the fine grain size, a large number of nanoscale second phases precipitating from the matrix are another important factor. Moreover, the Nd addition gives rise to the improvement of elongation of the extruded alloys, which is uncommon to previous studies [8,9]. Hence, the best tensile properties appear in the extruded Mg−9Gd−2Nd−0.5Zr alloy (YS=(320.7±6.3) MPa, UTS=(372.2±6.1) MPa, EL=(31.3±1.8)%). It is interesting that the elongation of the as-cast alloys decreases after Nd addition, while the extruded alloys present the opposite trend. This is because bulky network $Mg_5$(Gd, Nd) phases are formed after Nd addition, resulting in stress concentration

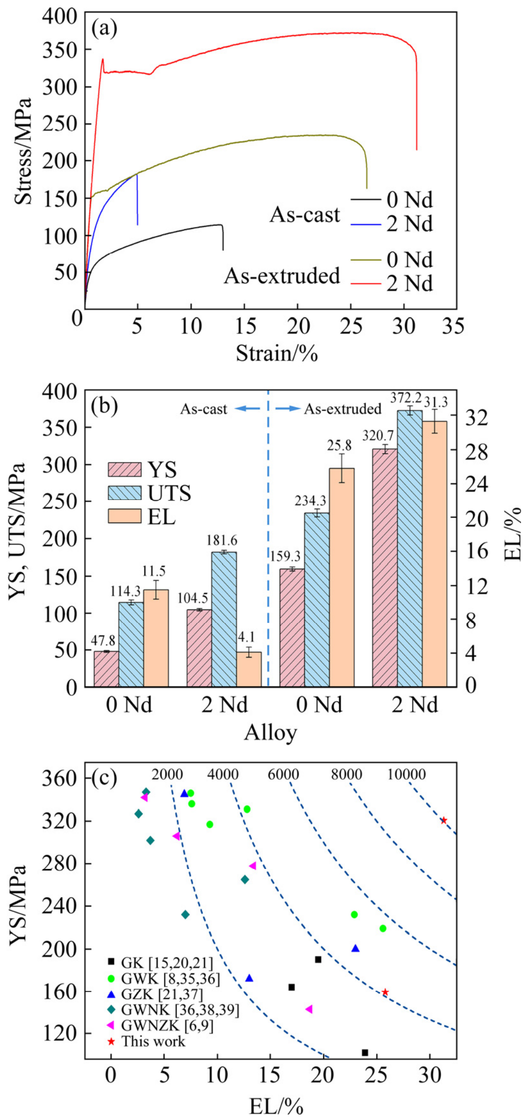


**Fig. 8** Tensile stress−strain curves (a), and tensile properties (b) of as-cast and extruded alloys; yield strength and elongation of wrought Mg−Gd alloys (c) (Data 2000−10000 are product of YS and EL with unit of MPa•%)

between the second phase and $\alpha$-Mg matrix. However, in the extruded Mg−9Gd−2Nd−0.5Zr alloy, a large number of nano precipitates precipitated at the grain boundaries, which did not cause stress concentration. And, the texture plays an important role in improving the ductility of alloys. With the addition of Nd, the RE texture component ([$\bar{1}2\bar{1}1$]) was formed and the maximum intensity of the texture decreased from 5.66 to 1.86, which was a soft orientation resulting in an increase in elongation. Figure 8(c) shows the tensile mechanical properties of wrought Mg−Gd alloys, including this work. It is obvious that the alloy fabricated in this study has superior comprehensive properties compared with the Mg−Gd based alloys reported previously [6,8,9,15,20,21,35−39], which has an excellent strength−elongation multiplier larger than 10000 MPa·%.

In order to study the improvement in YS between extruded Mg−9Gd−0.5Zr and Mg−9Gd−2Nd−0.5Zr alloys, the grain refinement strengthening mechanism ($\sigma_{HP}$) and the precipitate strengthening mechanism ($\sigma_{Or}$) were considered. Because of the Nd addition, the grain size of extruded alloys is refined from 5.23 to 1.68 μm. In view of the famous Hall−Petch theory, $\sigma_{HP}$ should be calculated by the following equation [40,41]:

$$\sigma_{HP}=kd^{-1/2} \tag{2}$$

where $k$ is the Hall–Petch slope and $d$ is the average grain size. According to CHENG et al [42], the $k$ value is 280−320 MPa·μm$^{1/2}$ for Mg alloys. Based on the above observations, the calculated increment in YS owing to grain refinement is 100.32−114.65 MPa after adding Nd.

The dynamically precipitated nano particles are distributed at the grain boundaries. A focused ion beam (FIB) image of the particles is shown in Fig. 9. According to the EDS results (map and points), the black particles represent the $Mg_5(Gd,Nd)$ phase, which precipitates dynamically during extrusion. There are dislocations clustering around the dynamic precipitation, which are marked by a yellow circle. In addition, some dislocation loops are formed around the particles (marked as green dotted lines) after the dislocation bypasses the particles. This indicates that the dynamically precipitated nano-$Mg_5(Gd,Nd)$ particles are impenetrable obstacles, which can improve the strength by hindering the dislocation movement

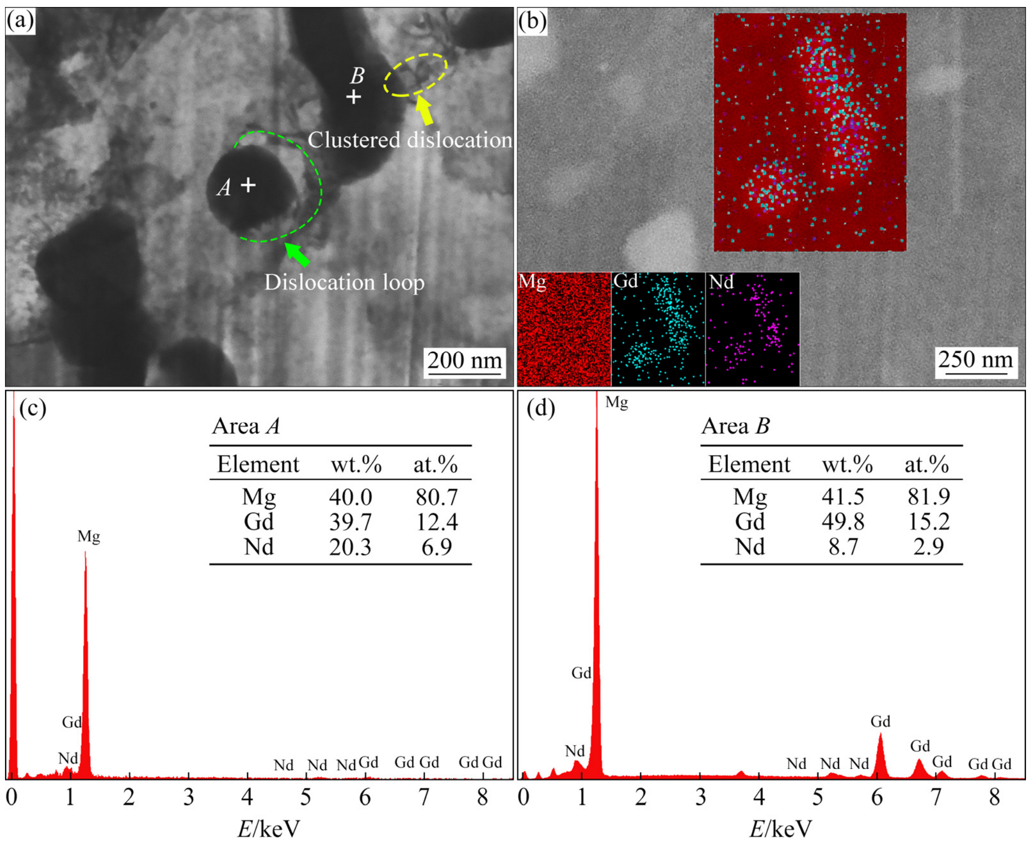


**Fig. 9** FIB morphology (a, b) and EDS analysis (c, d) of extruded Mg−9Gd−2Nd−0.5Zr alloy

through the Orowan strengthening mechanism. Therefore, the contribution of nano-$Mg_5$(Gd,Nd) particles to the YS can be calculated using the well-known Orowan hardening equation [43]:

$$\sigma_{\mathrm{Or}}=\frac{MGb}{2\pi(1-\upsilon)^{1/2}}\frac{1}{\lambda}\ln\frac{d_{\mathrm{p}}}{r_0} \tag{3}$$

where $M$ is the Taylor factor taking value of the inverse of the measured Schmid factor (SF), $G$ is the shear modulus of Mg ($G$=17.2 GPa [44]), $b$ is the magnitude of Burgers vector ($b$=0.32 nm [44]), $d_{\mathrm{p}}$ represents the mean diameter of precipitate, $v$ is the Poisson ratio ($v$=0.35 [44]), $r_0$ is the inner cut-off radius of the dislocation, equal to $b$ [45], and $\lambda$ represents the spacing between planar inter-obstacles. The precipitated $Mg_5$(Gd,Nd) particles can be regarded as nearly spherical and $\lambda$ can be calculated by [43]

$$\lambda=(0.779/f_{\mathrm{p}}^{1/2}-0.785)d_{\mathrm{p}}/2 \tag{4}$$

where $f_{\mathrm{p}}$ is the volume fraction of precipitates. In this research, $f_{\mathrm{p}}$ and $d_{\mathrm{p}}$ were surveyed from the high-resolution SEM images using the ImageJ software. Based on the statistics, $d_{\mathrm{p}}$ and $f_{\mathrm{p}}$ are 260 nm and 10.4%, respectively. According to the calculation, the contribution of the second phase to the yield strength is approximately 52.28 MPa. Consequently, the sum of calculations from the two strengthening mechanisms is commensurate with the experimental results (161.4 MPa), which indicates that the increase in the YS of the as-extruded Mg−9Gd−0.5Zr alloy with Nd addition mainly comes from grain refinement strengthening and precipitate strengthening.

The fracture surfaces of the Mg−9Gd−(2Nd)−0.5Zr alloys before and after extrusion are exhibited in Fig. 10. The fracture surfaces of the as-cast Mg−9Gd−(2Nd)−0.5Zr alloys contain dimpled regions, cleavage facets, particles and cracks, marked as $A$, $B$, $C$ and $D$, respectively. The dimple regions decrease after adding Nd, while the cleavage facets increase. The cracks are always accompanied by particles, indicating that the second phase is the origin of microcracks because of the stress concentration between the $\alpha$-Mg matrix and second phase [46,47]. Because of more and larger second phases, the Mg−9Gd−2Nd−0.5Zr alloy shows lower plasticity. However, after extrusion, the fracture surfaces of the alloys contain only dimpled regions and numerous tiny particles, which is consistent with their competitive elongation. Moreover, Fig. 10(d) exhibits that the dimples of Mg−9Gd−2Nd−0.5Zr alloy are smaller than those of Mg−9Gd−0.5Zr alloy.

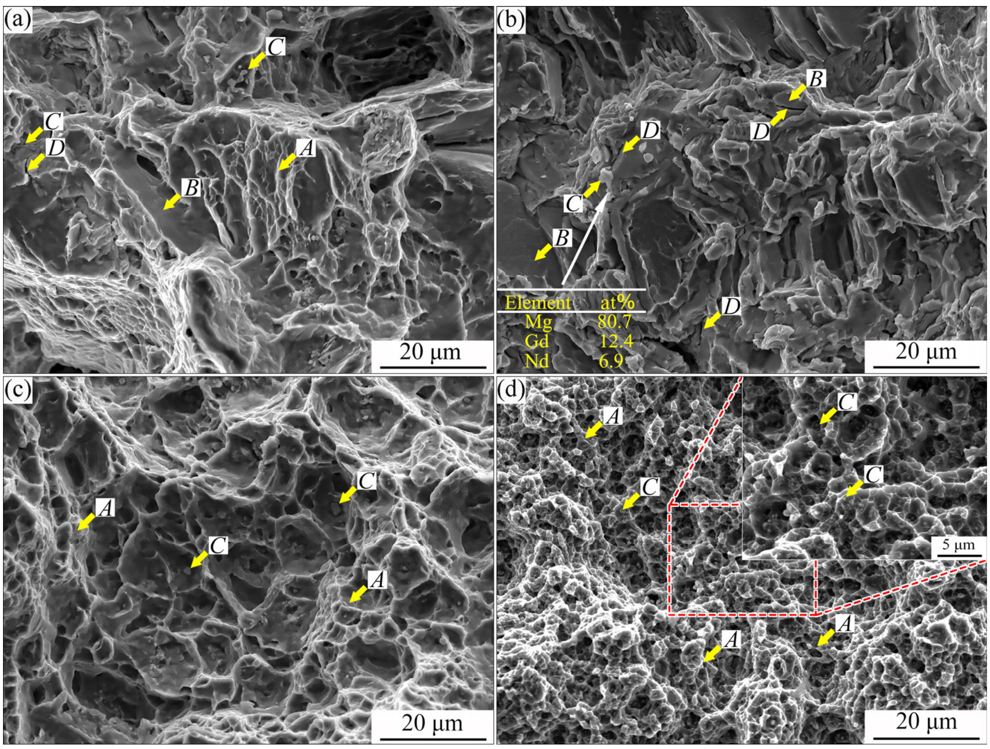


**Fig. 10** Fracture surfaces of alloys after tensile tests: (a) As-cast Mg−9Gd−0.5Zr; (b) As-cast Mg−9Gd−2Nd−0.5Zr; (c) As-extruded Mg−9Gd−0.5Zr; (d) As-extruded Mg−9Gd−2Nd−0.5Zr

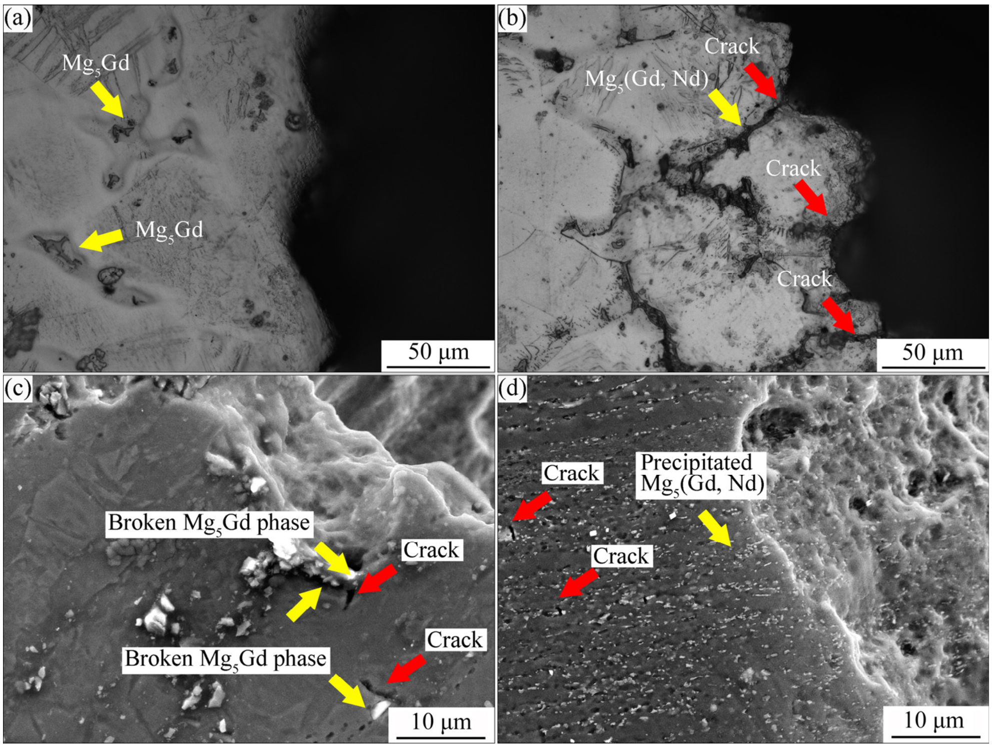


**Fig. 11** OM images (a, b) and SEM images (c, d) of longitudinal section of tensile fracture specimen: (a) As-cast Mg−9Gd−0.5Zr; (b) As-cast Mg−9Gd−2Nd−0.5Zr; (c) As-extruded Mg−9Gd−0.5Zr; (d) As-extruded Mg−9Gd−2Nd−0.5Zr

In order to further detect the fracture mechanism of Mg−9Gd−(2Nd)−0.5Zr alloys, tensile fracture specimens were observed in the longitudinal direction by OM and SEM (Fig. 11). The as-cast alloys are observed by OM because of the large second phase and grain size. The as-extruded alloys are observed by SEM due to the fine second phase and grain size. As can be seen from Fig. 11(b), the cracks initiate from the large $Mg_5$(Gd,Nd) phase, which indicates that the bulky second phase is the origin of microcracks [48]. This result is consistent with the observation of the fracture surface (Fig. 10(b)). Therefore, the as-cast Mg−9Gd−2Nd−0.5Zr alloy has the worst ductility. For the as-extruded alloys, it is difficult to observe the generation of cracks due to the fine second phases, especially in the as-extruded Mg−9Gd−2Nd−0.5Zr alloy. Hence, the alloys obtain better ductility after extrusion. However, in the as-extruded Mg−9Gd−0.5Zr alloy, there are a small amount of larger micron second phases resulting in the generation of cracks, which leads to a lower ductility compared with the as-extruded Mg−9Gd−2Nd−0.5Zr alloy. Another reason why the best ductility is obtained in the as-extruded Mg−9Gd−2Nd−0.5Zr alloy is that the RE texture $[1\bar{2}11]$ is formed after extrusion, which promotes the prismatic slip.

## 4 Conclusions

(1) The second phase in the as-cast Mg−9Gd−0.5Zr alloy is the $Mg_5Gd$ phase. After adding Nd, the $Mg_5Gd$ phase is changed into the $Mg_5$(Gd,Nd) phase, which means that some Gd in $Mg_5Gd$ is replaced by Nd.

(2) The Mg−9Gd−0.5Zr alloy exhibits a bimodal microstructure consisting of fine DRXed grains with RE texture and elongated un-DRXed grains with strong basal texture after extrusion. While, the microstructure of the Mg−9Gd−2Nd−0.5Zr alloy is only composed of uniform and fine DRXed grains. Therefore, the texture intensity decreases after adding Nd.

(3) After extrusion, the strength and elongation of the Mg−9Gd−(2Nd)−0.5Zr alloys increase simultaneously. In addition, the Nd addition gives rise to the improvement of strength and ductility. Thus, the as-extruded Mg−9Gd−2Nd−0.5Zr alloy possesses the best tensile properties (YS=

(320.7±6.3) MPa, UTS=(372.2±6.1) MPa, EL=(31.3±1.8)%).

(4) According to the calculation, the increase in the YS of the as-extruded Mg−9Gd−0.5Zr alloy due to Nd addition mainly comes from the grain refinement strengthening and precipitate strengthening.

## Acknowledgments

This work was supported by the Natural Science Foundation of Shanxi Province, China (Nos. 20210302123135, 20210302123163, 201901D211096, 201901D111272), Youth Program of National Natural Science Foundation of China (No. 51901153), Science and Technology Major Project of Shanxi Province, China (Nos. 20191102008, 20191102007, 20191102004), and Shanxi Province Scientific Facilities and Instruments Shared Service Platform of Magnesium-based Materials Electric Impulse Aided Forming, China (No. 201805D141005).

## References

[1] DING Zhi-bing, ZHAO Yu-hong, LU Ruo-peng, YUAN Mei-ni, WANG Zhi-jun, LI Hui-jun, HOU Hua. Effect of Zn addition on microstructure and mechanical properties of cast Mg−Gd−Y−Zr alloys [J]. Transactions of Nonferrous Metals Society of China, 2019, 29(4): 722−734.

[2] GAO Lei, CHEN Rong-shi, HAN En-hou. Enhancement of ductility in high strength Mg−Gd−Y−Zr alloy [J]. Transactions of Nonferrous Metals Society of China, 2011, 21(4): 863−868.

[3] LIU Huan, SUN Chao, WANG Ce, LI Yu-hua, BAI Jing, XUE Feng, MA Ai-bin, JIANG Jing-hua. Improving toughness of a $Mg_2Ca$-containing Mg−Al−Ca−Mn alloy via refinement and uniform dispersion of $Mg_2Ca$ particles [J]. Journal of Materials Science & Technology, 2020, 59: 61−71.

[4] CAO Fu-yong, ZHANG Jing, LI Ke-ke, SONG Guang-ling. Influence of heat treatment on corrosion behavior of hot rolled $Mg_5Gd$ alloys [J]. Transactions of Nonferrous Metals Society of China, 2021, 31(4): 939−951.

[5] MIRZADEH H. Quantification of the strengthening effect of rare earth elements during hot deformation of Mg−Gd−Y−Zr magnesium alloy [J]. Journal of Materials Research and Technology, 2016, 5(1): 1−4.

[6] HOU X L, PENG Q M, CAO Z Y, XU S W, KAMADO S, WANG L D, WU Y M, WANG L M. Structure and mechanical properties of extruded Mg−Gd based alloy sheet [J]. Materials Science and Engineering A, 2009, 520: 162−167.

[7] BAYAT-TORK N, MAHMUDI R, HOSEINI-ATHAR M M. Hot deformation constitutive analysis and processing maps of extruded Mg−Gd binary alloys [J]. Journal of Materials Research and Technology, 2020, 9(6): 15346−15359.

[8] YU Z J, XU C, MENG J, LIU K, FU J L, KAMADO S. Effects of extrusion ratio and temperature on the mechanical properties and microstructure of as-extruded Mg−Gd−Y−(Nd/Zn)−Zr alloys [J]. Materials Science and Engineering A, 2019, 762: 138080.

[9] YU Z J, HUANG Y D, QIU X, WANG G F, MENG F Z, HORT N, MENG J. Fabrication of a high strength Mg−11Gd−4.5Y−1Nd−1.5Zn−0.5Zr (wt%) alloy by thermomechanical treatments [J]. Materials Science and Engineering A, 2015, 622: 121−130.

[10] LIU L Z, CHEN X H, PAN F S, GAO S Y, ZHAO C Y. A new high-strength Mg−Zn−Ce−Y−Zr magnesium alloy [J]. Journal of Alloys and Compounds, 2016, 688: 537−541.

[11] BOHLEN J, YI S B, SWIOSTEK J, LETZIG D, BROKMEIER H G, KAINER K U. Microstructure and texture development during hydrostatic extrusion of magnesium alloy AZ31 [J]. Scripta Materialia, 2005, 53: 259−264.

[12] BALL E A, PRANGNELL P B. Tensile-compressive yield asymmetries in high strength wrought magnesium alloys [J]. Scripta Metallurgica et Materialia, 1994, 31: 111−116.

[13] STANFORD N, BARNETT M. Effect of composition on the texture and deformation behaviour of wrought Mg alloys [J]. Scripta Materialia, 2008, 58: 179−182.

[14] MACKENZIE L W F, DAVIS B, HUMPHREYS F J, LORIMER G W. The deformation, recrystallisation and texture of three magnesium alloy extrusions [J]. Materials Science and Technology, 2007, 23: 1173−1180.

[15] STANFORD N, BARNETT M R. The origin of “rare earth” texture development in extruded Mg-based alloys and its effect on tensile ductility [J]. Materials Science and Engineering A, 2008, 496: 399−408.

[16] BAYAT TORK N, RAZAVI S H, SAGHAFIAN H, MAHMUDI R. Microstructural evolution and mechanical properties of the as-cast and extruded Mg−Gd alloys [J]. Advanced Engineering Materials, 2016, 18: 156−161.

[17] WU J, CHIU Y L, JONES I P. Effect of Gd on the microstructure of as-cast Mg−4.2Zn−0.8Y (at.%) alloys [J]. Journal of Alloys and Compounds, 2016, 661: 455−460.

[18] POURBAHARI B, MIRZADEH H, EMAMY M. Toward unraveling the effects of intermetallic compounds on the microstructure and mechanical properties of Mg−Gd−Al−Zn magnesium alloys in the as-cast, homogenized, and extruded conditions [J]. Materials Science and Engineering A, 2017, 680: 39−46.

[19] CHEN X Y, LI Q A, ZHU L M, ZHANG S, WANG S B, GUAN H K. Tensile creep behavior and microstructure evolution of Mg−11Gd−2Y−0.5Zr alloy [J]. Vacuum, 2019, 167: 421−427.

[20] LI R G, NIE J F, HUANG G J, XIN Y C, LIU Q. Development of high-strength magnesium alloys via combined processes of extrusion, rolling and ageing [J]. Scripta Materialia, 2011, 64: 950−953.

[21] LIU K, ZHANG J H, ROKHLIN L L, ELKIN F M, TANG D X, MENG J. Microstructures and mechanical properties of extruded Mg−8Gd−0.4Zr alloys containing Zn [J]. Materials Science and Engineering A, 2009, 505: 13−19.

[22] ROKHLIN L L, DOBATKINA T V, NIKITINA N I.

Constitution and properties of the ternary magnesium alloys containing two rare-earth metals of different subgroups [J]. Materials Science Forum, 2003, 419/420/421/422: 291−296.

[23] HAO Mei-juan, CHENG Wei-li, WANG Li-fei, MOSTAED E, BIAN Li-ping, WANG Hong-xia, NIU Xiao-feng. Texture evolution induced by twinning and dynamic recrystallization in dilute Mg−1Sn−1Zn−1Al alloy during hot compression [J]. Journal of Magnesium and Alloys, 2020, 8: 899−909.

[24] BOHLEN J, YI S B, LETZIG D, KAINER K U. Effect of rare earth elements on the microstructure and texture development in magnesium−manganese alloys during extrusion [J]. Materials Science and Engineering A, 2010, 527: 7092−7098.

[25] CHEN Q W, TANG A T, YE J H, HAO L L, WANG Y R, ZHANG T J. Equilibrium and metastable phases in a designed precipitation hardenable Mg−3Gd−3Nd−0.6Zr alloy [J]. Materials Science and Engineering A, 2017, 686: 26−33.

[26] ZHU S M, NIE J F, GIBSON M A, EASTON M A. On the unexpected formation of rare earth hydrides in magnesium−rare earth casting alloys [J]. Scripta Materialia, 2014, 77: 21−24.

[27] WANG X Y, LI W Y, MA T J, YANG X W, VAIRIS A, TAO J. Microstructural heredity and its effect on mechanical properties of linear friction welded Ti−6.5Al−3.5Mo−1.5Zr−0.3Si alloy joints [J]. Materials Characterization, 2020, 168: 110540.

[28] PENG Q M, WU Y M, FANG D Q, MENG J, WANG L M. Microstructures and mechanical properties of Mg−8Gd−0.6Zr−$x$Nd ($x$=0, 1, 2 and 3 mass%) alloys [J]. Journal of Materials Science, 2007, 42: 3908−3913.

[29] SHENG L Y, ZHANG X R, ZHAO H, DU B N, ZHENG Y F, XI T F. Influence of multi-pass hot extrusion on microstructure and mechanical properties of the Mg−4Zn−1.2Y−0.8Nd alloy [J]. Crystals, 2021, 11(4): 425−438.

[30] HALLBERG H. Approaches to modeling of recrystallization [J]. Metals, 2011, 1: 16−48.

[31] GOURDET S, MONTHEILLET F. An experimental study of the recrystallization mechanism during hot deformation of aluminium [J]. Materials Science and Engineering A, 2000, 283: 274−288.

[32] ROBSON J D, HENRY D T, DAVIS B. Particle effects on recrystallization in magnesium−manganese alloys: Particle-stimulated nucleation [J]. Acta Materialia, 2009, 57: 2739−2747.

[33] BOHLEN J, NÜRNBERG M R, SENN J W, LETZIG D, AGNEW S R. The texture and anisotropy of magnesium−zinc−rare earth alloy sheets [J]. Acta Materialia, 2007, 55: 2101−2112.

[34] DU B N, HU Z Y, WANG J L, SHENG L Y, ZHAO H, ZHENG Y F, XI T F. Effect of extrusion process on the mechanical and in vitro degradation performance of a biomedical Mg−Zn−Y−Nd alloy [J]. Bioactive Materials, 2020, 5: 219−227.

[35] HE S M, ZENG X Q, PENG L M, GAO X, NIE J F, DING W J. Microstructure and strengthening mechanism of high strength Mg−10Gd−2Y−0.5Zr alloy [J]. Journal of Alloys and Compounds, 2007, 427: 316−323.

[36] YU Z J, XU C, MENG J, ZHANG X H, KAMADO S. Microstructure evolution and mechanical properties of as-extruded Mg−Gd−Y−Zr alloy with Zn and Nd additions [J]. Materials Science and Engineering A, 2018, 713: 234−243.

[37] YAMASAKI M, ANAN T, YOSHIMOTO S, KAWAMURA Y. Mechanical properties of warm extruded Mg−Zn−Gd alloy with coherent 14H long periodic stacking ordered structure precipitate [J]. Scripta Materialia, 2005, 53: 799−803.

[38] XIA X S, WANG C P, WU Y, ZHANG K, MA M L, YUAN B G. Grain refinement, microstructure and mechanical properties homogeneity of Mg−Gd−Y−Nd−Zr alloy during multidirectional forging [J]. Journal of Materials Engineering and Performance, 2018, 27: 5689−5699.

[39] LIU X, HU W Y, LE Q C, ZHANG Z Q, BAO L, CUI J Z. Microstructures and mechanical properties of high performance Mg−6Gd−3Y−2Nd−0.4Zr alloy by indirect extrusion and aging treatment [J]. Materials Science and Engineering A, 2014, 612: 380−386.

[40] YU Hui-hui, XIN Yun-chang, WANG Mao-yin, LIU Qing. Hall−Petch relationship in Mg alloys: A review [J]. Journal of Materials Science & Technology, 2018, 34: 248−256.

[41] QIAN Chen-hao, HE Zi-yang, LIANG Cheng, JI Wei-xi. Microstructure and hardness of W−25Re alloy processed by high-pressure torsion [J]. Transactions of Nonferrous Metals Society of China, 2017, 27: 2622−2629.

[42] CHENG W L, TIAN Q W, YU H, ZHANG H, YOU B S. Strengthening mechanisms of indirect-extruded Mg−Sn based alloys at room temperature [J]. Journal of Magnesium and Alloys, 2014, 2: 299−304.

[43] NIE J F. Effects of precipitate shape and orientation on dispersion strengthening in magnesium alloys [J]. Scripta Materialia, 2003, 48: 1009−1015.

[44] ROBSON J D, PAA-RAI C. The interaction of grain refinement and ageing in magnesium-zinc-zirconium (ZK) alloys [J]. Acta Materialia, 2015, 95: 10−19.

[45] HUTCHINSON C R, NIE J F, GORSSE S. Modeling the precipitation processes and strengthening mechanisms in a Mg−Al−(Zn) AZ91 alloy [J]. Metallurgical and Materials Transactions A: Physical Metallurgy and Materials Science, 2005, 36: 2093−2105.

[46] DU B N, XIAO Z P, QIAO Y X, ZHENG L, YU B Y, XU D K, SHENG L Y. Optimization of microstructure and mechanical property of a Mg−Zn−Y−Nd alloy by extrusion process [J]. Journal of Alloys and Compounds, 2019, 775: 990−1001.

[47] HOU Cai-hong, YE Zhi-song, QI Fu-gang, WANG Qing, LI Lian-hui, OUYANG Xiao-ping, ZHAO Nie. Effect of Al addition on microstructure and mechanical properties of Mg−Zn−Sn−Mn alloy [J]. Transactions of Nonferrous Metals Society of China, 2021, 31: 1951−1968.

[48] SHENG L Y, DU B N, HU Z Y, QIAO Y X, XIAO Z P, WANG B J, XU D K, ZHENG Y F, XI T F. Effects of annealing treatment on microstructure and tensile behavior of the Mg−Zn−Y−Nd alloy[J]. Journal of Magnesium and Alloys, 2020, 8(3): 601−613.

# Nd 添加结合热挤压制备 Mg−Gd−Zr 合金的力学性能

郑留伟[1]，庄永鹏[1]，李军舰[1]，王红霞[1]，李 航[1]，侯 华[2]，王利飞[1]，罗小平[1]，Kwang Seon SHIN[3]

1. 太原理工大学 材料科学与工程学院，山西省先进镁基材料重点实验室，太原 030024；
2. 中北大学 材料科学与工程学院，太原 030051；
3. Magnesium Technology Innovation Center, School of Materials Science and Engineering, Seoul National University, Seoul-08826, Korea

**摘 要：**研究添加钕元素对挤压态 Mg−9Gd−0.5Zr(质量分数，%)合金显微组织和力学性能的影响。在 673 K 下对 Mg−9Gd−0.5Zr 和 Mg−9Gd−2Nd−0.5Zr 两种合金进行挤压。添加钕后，组织中被拉长的非动态再结晶晶粒消失，获得均匀分布的动态再结晶晶粒，晶粒尺寸为 1.68 μm。此外，在挤压态 Mg−9Gd−2Nd−0.5Zr 合金中动态析出大量的纳米 $Mg_5$(Gd, Nd)颗粒，通过 Orowan 强化机制有效地提高合金的强度。细小的纳米颗粒通过阻碍形变能的释放为动态再结晶过程提供形核，进一步促进动态再结晶的进行。而且，动态再结晶晶粒具有弱织构，对塑性的提高起重要作用。因此，添加钕能够同时提高挤压态 Mg−9Gd−0.5Zr 合金的强度和伸长率。

**关键词：**Mg–Gd 基合金；热挤压；动态再结晶行为；织构；力学性能

**(Edited by Xiang-qun LI)**